Computer-Aided Design ▮ (▮▮▮▮) ▮▮▮–▮▮▮

Contents lists available at SciVerse ScienceDirect

Computer-Aided Design

journal homepage: www.elsevier.com/locate/cad

Geometry guided crystal phase transition pathway search

Edin Crnkic, Lijuan He, Yan Wang*

Woodruff School of Mechanical Engineering, Georgia Institute of Technology, 813 Ferst Drive NW, Atlanta, GA 30332-0405, United States

ARTICLE INFO

Keywords:
Computer-aided nano-design
Implicit modeling
Phase transition

ABSTRACT

Recently a periodic surface model was developed to assist geometric construction in computer-aided nano-design. This implicit surface model helps create super-porous nano structures parametrically and supports crystal packing. In this paper, we propose a new approach for pathway search in phase transition simulation of crystal structures. The approach relies on the interpolation of periodic loci surface models. Respective periodic plane models are reconstructed from the positions of individual atoms at the initial and final states, and surface correspondences are found. With geometric constraints imposed based on physical and chemical properties of crystals, two surface interpolation methods are used to approximate the intermediate atom positions on the transition pathway in the full search of the minimum energy path. This hybrid approach integrates geometry information in the configuration space and physics information to allow for an efficient transition pathway search. The methods are demonstrated by examples of FeTi, VO_2, and FePt.

1. Introduction

With the observation that hyperbolic surfaces exist in nature ubiquitously and periodic features are common in condensed materials, we recently proposed an implicit surface modeling approach, periodic surface (PS), to represent geometric structures at nano scales [1]. Periodic surfaces are applied as either loci or foci in geometry construction. Loci surfaces are fictional continuous surfaces that pass through discrete particles in 3-dimensional (3D) space, whereas foci surfaces can be regarded as isosurfaces of potential or density in which discrete particles are enclosed. The surface model allows for parametric construction of highly porous structures from atomic scale to meso scale. A new feature-based approach to construct crystal structures based on loci surfaces was proposed [2]. Reconstruction of loci surfaces from crystals [3], complexity control [4], and Minkowski sum [5] of PS models were also studied.

In addition, we developed a metamorphosis approach based on foci surfaces that models the structural change in phase transitions [6]. A phase transition is a geometric and topological transformation process of materials from one phase to another, each of which has a unique and homogeneous physical property. Understanding and controlling phase transition is critical in designing various functional materials, such as for information storage (e.g. magnetic disk, phase-change memory, CD-ROM) and energy storage (e.g. battery, shape-memory alloy, solid-state materials for hydrogen storage). More generally, a tool which allows engineers to visualize and gather information about phase transitions would be an asset for the application of the functional materials as part of a solution to engineering problems. The creation of such a tool is the motivation behind the research presented in this paper.

Traditionally, phase transition is described from a top-down viewpoint as the transformation of a thermodynamic system from one phase to another. A phase is a state where all physical properties are uniform throughout the material, and the system has a particular level of free energy. When external conditions are altered, such as a change in temperature or pressure, one or more properties of the material change and a phase transition occurs. The system moves from one free energy level to another as a result of these external influences. The external conditions and the amount of energy input required are quantitative measures that are used to define the phase transition. It is not necessary for the material to undergo a change in its state of matter, for example from liquid to solid. Material properties can change while remaining in the same state throughout the transition. Yet the complete understanding of phase transitions is not available, even the classifications of first-, second-, and infinite-order [7,8].

Phase transition describes a wide variety of processes in diverse domains, such as liquid, ferromagnetic, superconducting, and others. In this paper, we take a bottom-up viewpoint and refer to phase changes as geometric and topological reconfiguration, rather than the top-down classical thermodynamic viewpoint. With this approach, we are interested in changes in the material structure on an atomic scale. Structural changes in phase transitions have been found to be more common than previously thought. For instance, ferromagnetic phase transition was recently found to be related

* Corresponding author. Tel.: +1 404 894 4714; fax: +1 404 894 9342.
E-mail address: yan.wang@me.gatech.edu (Y. Wang).

0010-4485/$ – see front matter © 2011 Elsevier Ltd. All rights reserved.
doi:10.1016/j.cad.2011.08.009

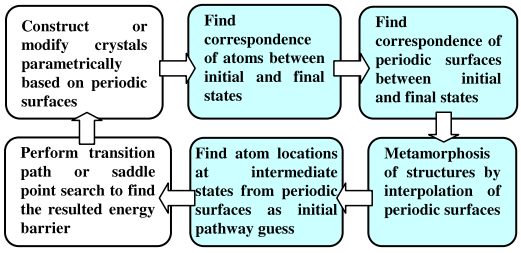

Fig. 1. Steps of computer-aided transition pathway design.

to crystal shape changes [9,10]. The modeling of materials and phase changes from this bottom-up viewpoint have been discussed frequently in literature (e.g. [11,12]). The purpose of this paper is to present a new geometry-guided approach to provide good initial guesses of the transition path for crystals aided by the PS models so that the model construction for design and the pathway search for first-principles simulation can be effectively integrated. Good initial guesses reduce the risk of being trapped in the paths of saddle points with local minimum energy. Thus the accuracy of the true pathway prediction can be improved.

In our metamorphosis approach, PS models of the start and end crystal structures are built based on loci surfaces. Loci surface construction is used because intersections of loci surfaces present a convenient method of defining atom locations in a crystal structure. A detailed investigation of basic crystal feature and crystal structure construction using this method can be found in previously published work [2]. The initial guess of the transition path is represented as the interpolation between the start and end PS models in the parameter space. We will present a method of finding the correspondence between atoms in the initial and final states and use this information to construct PS models. Two methods of PS model interpolation are also developed. Fig. 1 shows an outline of the foreseen computer-aided transition pathway design process. It is hoped that the closed-loop process can iteratively find a good design of materials structure and composition with the desirable transition rate. The shaded boxes show the new method presented in this paper.

In the remainder of the paper, Section 2 summarizes some existing methods and concepts in geometric modeling and transition pathway search as a background to our proposed methods. Section 3 gives an introduction of the periodic surface model. Section 4 provides an overview of our geometry-guided transition pathway search and describes the method of feature-based crystal construction. It also details the aforementioned morphing of surfaces between states. Section 5 discusses the searching of the surface correspondence based on a minimum energy change approach as well as constraints that can be applied. Section 6 gives demonstrations of the methods, and Section 7 summarizes the findings.

2. Background

The most important step involved in modeling phase transition is the knowledge of the activation energy barrier during the transition, which can be found by traversing the transition pathway. A number of methods already exist to search transition paths and saddle points on a potential energy surface (PES), where configurations with local minimal energy correspond to the stable or metastable states of the materials system. The energy difference between the initial state and the saddle point with the lowest possible energy barrier on a PES, which corresponds to the highest energy level along the minimum energy path (MEP), gives the estimate of the transition rate constant. The lower the energy difference is, the easier or faster the transition could be. Most of these pathway and saddle-point search methods, which will be summarized in Sections 2.2 and 2.3, rely on an initial guess of the transition path from the initial state (or phase) to the final one. The search usually is a local refinement process of which the final path passes through the saddle point with the lowest possible energy barrier. Thus the accuracy of these methods sensitively depends on the initial guesses of paths. Existing methods give the initial guesses by either simple linear interpolation of atoms' positions or case-by-case empirical approaches. New approaches systematically providing initial guesses that are reasonably close to the MEP are needed. In the remainder of this section, we present a brief summary of existing transition path and saddle point search methods and molecular scale geometric modeling techniques.

2.1. Geometric modeling of molecular structures

As part of research efforts in computer aided molecular design, modeling the geometry and topology of molecular structures has attracted researchers' attention. Edelsbrunner developed a novel method for modeling smooth surfaces based on skins specified by a set of weighted points [13]. Similarly, a method for reconstructing surfaces from a finite set of points was also proposed [14]. Bajaj et al. represented the surface boundary of molecules using a set of non-uniform rational B-spline patches [15]. Other efforts in geometry modeling include the construction of quality meshes for implicit salvation models of biomolecular structures [16] and computation and triangulation of the molecular surface of a protein with beta shapes [17–19]. Topology of ribbons [20], frequently used for modeling of DNA and proteins, was described in terms of the "knottiness" or link between two curves. An approach for computing the Euclidean Voronoi diagram for spheres [21] has also been presented. The Voronoi diagram was further used as a tool for meshing of particle systems within bounded regions [22].

2.2. Transition path search

Transition path search methods are classified either as chain-of-states methods, including nudged elastic band and string methods, or as one of the other methods. Chain-of-states methods rely on a collection of images that represent intermediate states of the atomic structure as it transforms from initial to final configurations along the transition path. These discrete states are chained to each other after the search converges, and the transition pathway and saddle point are obtained. The most common of these methods is the NEB [23], which relies on a series of images connected by springs. To increase the resolution at the region of interest (ROI) and the accuracy of saddle point energy estimates, the NEB method omits the perpendicular component of the spring force, as well as the parallel component of the true force due to the gradient of the potential energy. In some cases, this method produces paths with unwanted kinks, or may not have any images that are directly on the saddle point. The improved tangent NEB [24] and doubly nudged elastic band [25] methods reduce the appearance of kinks by generating a better estimate of the tangent direction of the path and re-introducing a perpendicular spring force component, respectively. Free-end NEB [26] only requires knowledge of either the initial or final state, rather than both, and climbing image NEB [27] allows the image with the highest energy to climb in order to locate the saddle point. Eigenvector following optimization can be applied to the result of NEB to locate actual saddle points, and the resolution of ROI can be increased by using adaptive spring constants [28].

String methods [29,30] represent the transition path continuously as splines that evolve and converge to the MEP. As opposed to NEB, the number of points used in the String method can be modified dynamically. The Growing String method [31] takes advantage of this by starting with points at the reactant and product, and then

Please cite this article in press as: Crnkic E, et al. Geometry guided crystal phase transition pathway search. Computer-Aided Design (2011), doi:10.1016/j.cad.2011.08.009

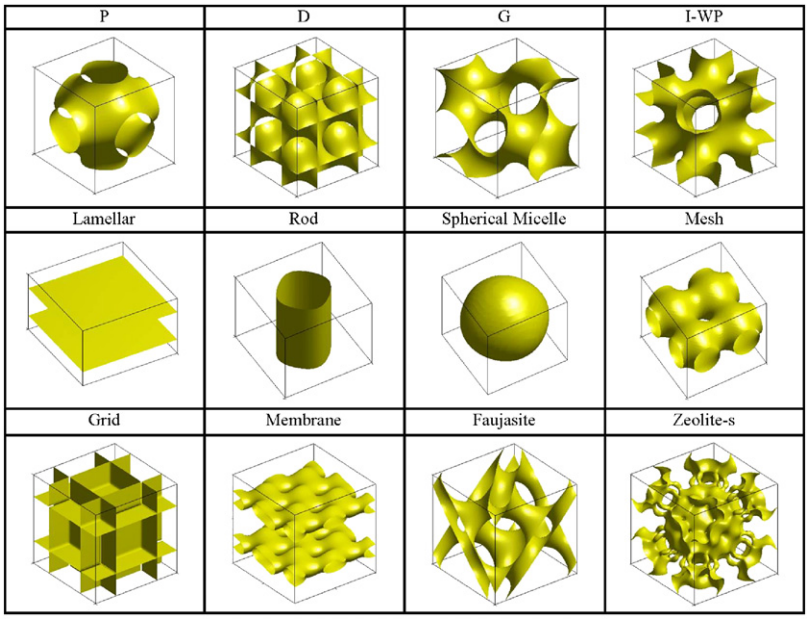

Fig. 2. Periodic surface models of cubic phase and mesophase structures.

adding points which meet at the saddle point. The Quadratic String method [32] is a variation that uses a multi-objective optimization approach.

Methods that are not classified as chain-of-states include the accelerated Langevin dynamics method [33] and the conjugate peak refinement method [34], which finds saddle points and the MEP by searching the maximum of one direction and the minima of all other conjugate directions iteratively. The Hamilton–Jacobi method [35] relies on the solution of a Hamilton–Jacobi type equation to generate the MEP.

2.3. Saddle point search

Instead of searching the complete MEP, saddle point search methods only locate the saddle point on the MEP. They are categorized into local and global search methods. One of the original local methods is the automated surface walking algorithm [36,37]. It is based on eigenvectors of the Hessian matrix with local quadratic approximations of the PES. The more recent ridge method [38] and dimer method [39] use a pair of images to search for the saddle point. Reduced Gradient Following [40] and Reduced Potential Energy Surface Model [41] methods use intersections of zero-gradient curves and surfaces, with saddle point search occurring within the subspace of these curves or surfaces. Finally, the Synchronous Transit method [42] estimates the transition state and refines the saddle point estimate through conjugate gradient optimization.

Local search methods may locate the saddle point which does not have the maximum energy on the MEP if there are multiple saddle points. Global search methods have the advantage that the saddle point with the maximum energy is located if the search converges. The Dewar–Healy–Stewart method [43] searches for the saddle point by iteratively reducing the distance between reactant and product images. The Activation–Relaxation technique [44] can travel between many saddle points using a two step process; an image first jumps from a local minimum to a saddle point, and then back down to another minimum. The Step and Slide method [45] uses an image from the initial and final state. Energy levels of each are increased gradually, and the distance between them is minimized while remaining on the same isoenergy surface. The interval Newton's method [46] is capable of finding all stationary points by solving the equation of vanishing gradient.

The proposed geometry guided approach in this paper is to provide an initial guess of the transition pathway that is reasonably close to the MEP in order to accelerate the searching of the chain-of-state methods, particularly the widely used climbing image NEB method. The geometry of crystals is constructed by a periodic surface model. The initial guess is computed by the metamorphosis of the surface model.

3. Periodic surface model

The periodic surface model has the implicit form and is defined as

$$\psi(\mathbf{r}) = \sum_{l=1}^{L}\sum_{m=1}^{M} \mu_{lm} \cos(2\pi\kappa_l(\mathbf{p}_m^T \cdot \mathbf{r})) = 0 \tag{1}$$

where κ_l is the scale parameter, $\mathbf{p}_m = [a_m, b_m, c_m, \alpha_m]^{\mathrm{T}}$ is a basis vector, such as one of

$$\{\mathbf{e}_0, \mathbf{e}_1, \mathbf{e}_2, \mathbf{e}_3, \mathbf{e}_4, \mathbf{e}_5, \mathbf{e}_6, \mathbf{e}_7, \mathbf{e}_8, \mathbf{e}_9, \mathbf{e}_{10}, \mathbf{e}_{11}, \mathbf{e}_{12}, \mathbf{e}_{13}, \ldots\}$$
$$= \left\{ \begin{bmatrix}0\\0\\0\\1\end{bmatrix} \begin{bmatrix}1\\0\\0\\1\end{bmatrix} \begin{bmatrix}0\\1\\0\\1\end{bmatrix} \begin{bmatrix}0\\0\\1\\1\end{bmatrix} \begin{bmatrix}1\\1\\0\\1\end{bmatrix} \begin{bmatrix}1\\0\\1\\1\end{bmatrix} \begin{bmatrix}0\\1\\1\\1\end{bmatrix} \begin{bmatrix}1\\1\\1\\1\end{bmatrix} \right.$$
$$\left. \begin{bmatrix}1\\-1\\0\\1\end{bmatrix} \begin{bmatrix}-1\\0\\1\\1\end{bmatrix} \begin{bmatrix}0\\1\\-1\\1\end{bmatrix} \begin{bmatrix}1\\-1\\1\\1\end{bmatrix} \begin{bmatrix}-1\\1\\1\\1\end{bmatrix} \begin{bmatrix}1\\1\\-1\\1\end{bmatrix} \cdots \right\}$$

which represents a basis plane in the Euclidean space $\mathbb{R}^3$, $\mathbf{r} = [x, y, z, w]^{\mathrm{T}}$ is the location vector with homogeneous coordinates, and μ_{lm} is the periodic moment. We assume $w = 1$ if not explicitly specified. The degree of $\psi(\mathbf{r})$ in Eq. (1) is defined as the number of unique vectors in the basis vector set $\{\mathbf{p}_m\}$. The scale of $\psi(\mathbf{r})$ is defined as the number of unique scale parameters in $\{\kappa_l\}$. We can assume scale parameters are natural numbers ($\kappa \in \mathbb{N}$).

Fig. 2 lists some examples of periodic surface models. Triply periodic minimal surfaces, such as *P*-, *D*-, *G*-, and I-WP cubic morphologies that are frequently referred to in chemistry and

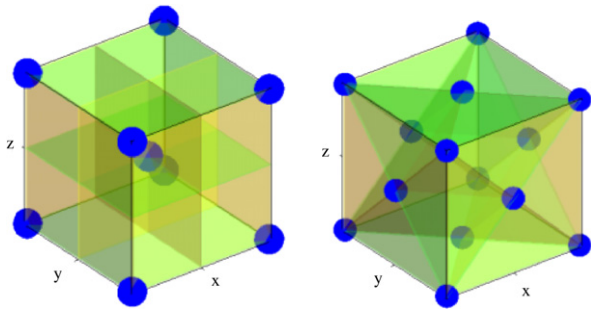

(a) Body-centered cubic. (a) Face-centered cubic.

Fig. 3. Body centered and face centered cubic structures constructed by loci periodic surfaces.

polymer literature, can be adequately approximated. Besides the cubic phase, other mesophase structures such as spherical micelles, lamellar, rod-like hexagonal phases can also be modeled. The lamellar structure, for example, can be represented as a periodic surface model using the equation

$$\cos(2\pi z) = 0 \tag{2}$$

and the *P*-structure is described using

$$\cos(2\pi x) + \cos(2\pi y) + \cos(2\pi z) = 0. \tag{3}$$

Equations corresponding to the other structures in Fig. 2 are more involved. They are discussed in greater detail in [1].

4. Loci surface model construction

The searching process in computer-aided transition pathway design starts with a unit cell of a crystal material in its initial state before it undergoes phase transition. The desirable locations of the atoms that make up this unit cell are known, and a loci surface model is reconstructed. Similarly, loci surface model reconstruction is also used for the final state to which the material will transition. The next step is to find intermediate steps between the known initial and final states. Using the atoms in the unit cell, the location of each atom in the initial state is compared to all the atoms in the final state. The correspondence between the states is determined based on the minimum distance approach or the minimum energy change, which will be discussed in Sections 4.2 and 4.3, respectively. Once it is known to which location each atom transitions, interpolation of corresponding PS models is used to find the atom locations at intermediate states. At each intermediate state, interpolated loci surfaces are used to model the geometry. Particularly for crystals, the simplest loci surfaces are periodic planes. This information about the geometric transition process of the unit cell, as a more accurate initial guess of the transition path, can be fed into the transition pathway search methods.

4.1. Crystal construction by loci surfaces

A process of tiling by intersection as described in [2] can be used to construct crystal structures. They are built with 14 Bravais lattices, each of which can be constructed via intersections of periodic surfaces. For three periodic surfaces $\psi_1(\mathbf{r}) = 0$, $\psi_2(\mathbf{r}) = 0$, $\psi_3(\mathbf{r}) = 0$, the intersection is found by solving $\psi(\mathbf{r}) = \psi_1^2(\mathbf{r}) + \psi_2^2(\mathbf{r}) + \psi_3^2(\mathbf{r}) = 0$. This provides a method for generating each of the points in a lattice. For instance, Fig. 3 shows a body centered and a face centered cubic structures. They are generated by

$$\cos^2(\pi(x - y + 0.5)) + \cos^2(\pi(x + y + 0.5)) + \cos^2(\pi(y + z + 0.5)) = 0 \tag{4}$$

and

$$\cos^2(\pi(x + y + z)) + \cos^2(\pi(-x + y + z)) + \cos^2(\pi(-x - y + z)) = 0 \tag{5}$$

respectively. The markers in the figure indicate atom positions generated by intersections of periodic surfaces. In the same way, all types of lattices can be constructed.

The most generic approach to reconstruct loci surface models from crystals is by constructing *y*–*z*, *x*–*z*, and *x*–*y* planes for each atom. Given a unit cell with the size of *a*, *b*, and *c* in the respective *x*, *y*, and *z* direction, the *y*–*z*, *x*–*z*, and *x*–*y* planes that go through the origin (0, 0, 0) have the respective basis vectors

$$\begin{cases} \mathbf{p}_{yz}(0) = [1, 0, 0, a/2] \\ \mathbf{p}_{xz}(0) = [0, 1, 0, b/2] \\ \mathbf{p}_{xy}(0) = [0, 0, 1, c/2] \end{cases} \tag{6}$$

and the respective scale parameters

$$\begin{cases} \kappa_x = 1/(2a) \\ \kappa_y = 1/(2b) \\ \kappa_o = 1/(2c). \end{cases} \tag{7}$$

If an atom in the unit cell has the coordinates *x*, *y*, and *z*, then the respective basis vectors for the *y*–*z*, *x*–*z*, and *x*–*y* planes that go through the atom are

$$\begin{cases} \mathbf{p}_{yz}(x) = [1, 0, 0, a/2 + x] \\ \mathbf{p}_{xz}(y) = [0, 1, 0, b/2 + y] \\ \mathbf{p}_{xy}(z) = [0, 0, 1, c/2 + z] \end{cases} \tag{8}$$

with the same scale parameters as in Eq. (7).

Obviously, when special knowledge about atoms is available, the periodic planes to construct atoms are not necessarily *y*–*z*, *x*–*z*, or *x*–*y* planes, such as the ones in Fig. 3(b). The number of planes can be reduced because of the correlation between atoms. Similar to Eq. (6), the information required to build a plane is the normal direction of the plane and its distance between the atom and the new origin of reference along the normal direction. For an atom in the unit cell with the coordinates *x*, *y*, and *z*, the basis vector of a periodic plane with the normal vector $\hat{n} = (n_x, n_y, n_z)$ (where $n_x^2 + n_y^2 + n_z^2 = 1$) is either $\mathbf{p}(x, y, z) = [n_x, n_y, n_z, a/2 - (n_x x + n_y y + n_z z)]$, $\mathbf{p}(x, y, z) = [n_x, n_y, n_z, b/2 - (n_x x + n_y y + n_z z)]$, or $\mathbf{p}(x, y, z) = [n_x, n_y, n_z, c/2 - (n_x x + n_y y + n_z z)]$ corresponding to the rotated plane with respect to *x*-, *y*-, or *z*-axis. The respective scale parameter for the plane is $\kappa = n_x/(2a)$, $\kappa = n_y/(2b)$, or $\kappa = n_z/(2c)$.

One important question that needs to be answered for the transition searching process is how atoms in initial and final states are corresponding to each other. Searching the correspondence between atoms is described in Section 4.2.

4.2. Searching correspondence of atoms

In general, there are two steps in modeling surface morphing. First, the location correspondence of atoms is identified. Then the PS models of the corresponding atoms are paired and the interpolation is made between them. To compare atom locations

between the initial and final states, we may use a matrix form for the locations, with rows 1, 2, and 3 containing the x, y, and z coordinates, respectively. For example, a cubic structure with one corner at $(0, 0, 0)$ and size of a, b, and c is represented by the matrix

$$\begin{bmatrix} 0 & a & a & 0 & 0 & a & a & 0 \\ 0 & 0 & b & b & 0 & 0 & b & b \\ 0 & 0 & 0 & 0 & c & c & c & c \end{bmatrix}.$$

It is assumed that each atom will transition to the nearest position in the final state. Data for atom locations in the final state is listed in a matrix with identical dimensions. Starting with the first column in the matrix of the initial phase, the Euclidean distance is calculated between this location and each location in the matrix of the final phase. The process is then repeated for all other columns in the initial matrix. The correspondence between locations in the initial and final phases is determined based on the minimum distance between them. That is, if $[q_1, \ldots, q_n]$ is the initial matrix containing n locations and the final matrix is $[q'_1, \ldots, q'_n]$, then the distance d_{ij} between the ith location in the initial matrix and the jth in the final one is $d_{ij} = |q_i - q'_j|$ where $1 \leq i \leq n$ and $1 \leq j \leq n$. For the ith location at the initial stage, the corresponding i_Fth location at the final stage is determined by

$$i_F = \arg \min_{1 \leq j \leq n} d_{ij}. \tag{9}$$

However, for complex crystal structures it becomes inconvenient to track all points individually. Inaccuracy can be introduced if there is a significant amount of rotation or scaling in the crystal, as the assumption may no longer be valid that each atom moves to the nearest position. Therefore, some improvements and simplifications can be introduced for certain structures. These include the classification approach described in Section 4.2.1 and the correlation approach introduced in Section 4.2.2.

4.2.1. Classification of positions

In many crystal structures, more than one type of element is present in the unit cell. In these cases it is not necessary to compare the locations of all atoms in the initial and final states because an atom of one element cannot move into a location occupied by a different element. The data in the location matrices needs to be sorted so that the atoms of each element are grouped together. In general, if certain atoms are not likely to be in certain positions, those positions can be excluded in the pair-wise comparison. The available positions are classified and grouped into several subsets. For example, in a body centered cubic structure, the first eight columns of the matrix can represent the corner atoms which are all the same element, and a final ninth column would represent the location of the central atom. Each atom in the initial configuration would then only be compared to atoms of the same element in the final phase, reducing the amount of computation needed in multi-element structures.

Suppose that there are a total of T different types of elements. The column indices of the location matrix can be grouped into T subsets as

$$(1, \ldots, n_1)(n_1 + 1, \ldots, n_2) \cdots (n_{t-1} + 1, \ldots, n_t) \cdots (n_{T-1} + 1, \ldots, n).$$

The computation of the minimal distance for type t element then is based on

$$i_F = \arg \min_{n_{t-1}+1 \leq j \leq n_t} d_{ij} \tag{10}$$

instead of Eq. (9).

4.2.2. Correlation of atoms

Depending on the types of bonds in the crystal, there may be groups of atoms that remain equidistant from each other on the same plane throughout the phase transition process. With graphite, for example, the bonds between carbon atoms along each plane are stronger than the bonds that connect planes to each other. The weaker bonds are more likely to separate, leaving the planes intact. This type of property can be taken into consideration when modeling the phase transition process. Atoms that are located on the same plane and remain in the same position relative to each other do not have to be considered individually during the process outlined in Section 4.2.1. Only the position of one of the atoms on the plane must be found, and the rest are placed in the same positions with respect to the coordinates of the first. This reduces the amount of computation when comparing atom coordinates because the corresponding position must be found for only one reference atom on the plane.

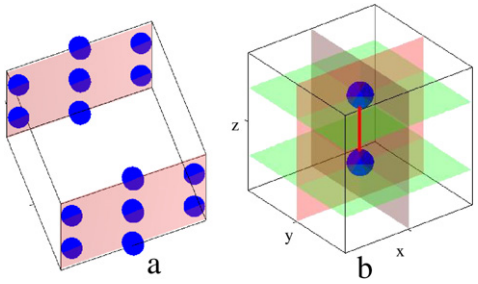

Fig. 4. Correlation of atoms: (a) hexagonal unit cell with face correlation, (b) two strongly bonded atoms with edge correlation.

In the graphite example, the structure can be modeled with hexagonal unit cells where atoms in the individual planes are connected with covalent bonds, while the planes are connected to each other by the van der Waals force. This indicates that atoms which are in the same plane are likely to remain on that plane. We call this special case *face correlation*. An example of a hexagonal structure is shown in Fig. 4(a) where the colored surfaces represent planes along which the atoms are covalently bonded. We can take advantage of these characteristics when modeling the structure by reducing the number of periodic surfaces required to construct it. Normally each of the 14 atoms in the unit cell of Fig. 4(a) would be represented by three perpendicular planes, meaning that the interpolation must be performed on 42 individual periodic surfaces. However, because the atoms in each layer have a common periodic surface, this number is reduced to 30. Two unique surfaces are required for each point, with the third being the common planes on the top and bottom of the hexagonal unit cell, shown in Fig. 4(a).

In cases where only two atoms have a bond that is stronger than other bonds in the structure, these atoms are less likely to break apart during the phase transition. The number of surfaces required for modeling can be reduced again because of shared intersection planes. The two planes that intersect to form the line along which the atoms are bonded are used to generate the locations of both atoms. Thus, instead of using six planes to model these two atoms, the number can be reduced to four. If the two atoms in Fig. 4(b) have a strong bond and can be assumed to remain in the same position relative to each other, they can be modeled using the four planes shown. The two vertical planes are common to both atoms. Their intersection represents the line along which the atoms are bonded. In addition, the two horizontal planes are used to define each atom's position along the z-axis. This special case of periodic surfaces is called *edge correlation*.

In summary, we find correspondence of atoms between initial and final states so that the respective periodic planes can be constructed. The interpolation of the planes then locates intermediate positions of atoms during the transition process. If all three planes for each atom are fully constructed, the correlation and energy exchange between atoms are ignored. Pair-wise comparison between

individual atoms is used in searching the correspondence, which is purely based on the geometry. Instead, if the number of planes is reduced because of the face correlation or edge correlation, the interaction among atoms is implicitly considered. Geometry and physics become more integrated. Yet, this atom correspondence approach assumes corresponding planes between initial and final states only translate during the transition process, whereas the rotation of planes is not considered. For instance, in the most general case, all planes are in either y–z, x–z, or x–y direction. A y–z plane in the initial state only translates to a y–z plane in the final state, similar for the other two. More importantly, when the number of planes increases, the exhaustive searching method of the atom correspondence becomes combinatorially expensive. In Section 4.3, we present a different approach to find the correspondence of periodic planes directly by a heuristic searching method without the need for computing the correspondence of atoms.

4.3. Correspondence of periodic planes by minimum potential energy change

Different from the atom correspondence method in Section 4.2 where each plane will simply move to the nearest available position, an alternative approach is to find the correspondence of planes directly by considering the total potential energy change of the system. We define the total potential energy change as a function of both displacement and rotation of each plane. The pair-wise correspondence between the initial and final planes is found by searching the minimum potential change. This method yields better results in more general structures where the planes undergo both rotation and translation. Since searching the global minimum of the potential energy change has the combinatorial complexity, heuristic optimization methods can be used for large systems. Here, we use a Monte Carlo simulation or simulated annealing (SA) like algorithm. The potential energy change is defined in Section 4.3.1, and the SA search algorithm is described in Section 4.3.2.

4.3.1. Translational and rotational potential change

As illustrated in Fig. 5, plane i used in the construction of a unit cell in the initial state is represented by a point and a vector, $\vec{a}_i$ and $\vec{p}_i$ respectively. If there are two or more atoms located on the plane, $\vec{a}_i$ can be placed at the center of the convex polygon formed by the atoms; otherwise it is simply placed at the location of the atom. $\vec{p}_i$ is a unit vector indicating the normal direction of the plane. Similarly, points $\vec{b}_i$ and vectors $\vec{q}_i$ are placed on the unit cell for the final state.

The points $\vec{a}_i$ and $\vec{b}_i$ are used to calculate the displacement of the planes. We use the Euclidean distance formula to find the distance d_i between $\vec{a}_i$ and $\vec{b}_i$, which is then used to find the translational potential change $\Delta V_i(d_i)$ between the two locations for pair i, given by

$$\Delta V_i(d_i) = s d_i^2 \tag{11}$$

where s is a constant coefficient.

In addition to the translational potential change, a rotational potential change is also defined for the transition of each plane. The angle θ_i between $\vec{p}_i$ and $\vec{q}_i$ is found and used to calculate the rotational potential change $\Delta U_i(\theta_i)$, given by

$$\Delta U_i(\theta_i) = c(1 - \cos(\theta_i)) \tag{12}$$

where c is a constant coefficient. $\Delta U_i(\theta_i)$ is added to $\Delta V_i(d_i)$ to receive the combined potential change for the plane's transition. In a structure with n planes, the total potential change is obtained by the summation of all planes as

$$\Delta W_{\text{total}} = \sum_{i=1}^{n} (\Delta U_i + \Delta V_i). \tag{13}$$

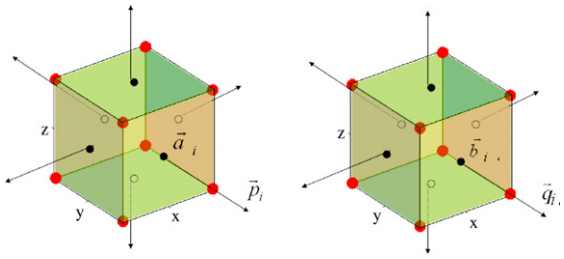

Fig. 5. Correspondence between locations and directions of planes.

Searching the correspondence of periodic planes is to find an arrangement with the minimum total potential change between the initial and final states. In each iteration, $\vec{a}_i$ and $\vec{p}_i$ remain unchanged, but they are used in combination with a different pair of $\vec{b}_i$ and $\vec{q}_i$ to find the total potential change. The combination that yields the lowest ΔW_{total} is used to determine to which location each plane transitions. After the correspondence between planes is determined, each of the atom locations in the final state is found using the intersection of the planes.

When the total number of planes is low such as in simple crystals, all combinations can be checked. For complex crystal structures with a large number of basis atoms in one unit cell, the effects of combinatorial complexity make it highly impractical to check all possible combinations. Even a structure with ten plane locations presents billions of possibilities. It becomes computationally expensive to go through more than a few thousand iterations, so a heuristic global optimization approach is preferred. The algorithm discussed in the following section provides a method of optimizing the solution without searching through all possible combinations. Although individual iterations of the algorithm are more involved than the simple exhaustive searching technique, the overall searching process is less computationally expensive for cases where the structure is more complex.

4.3.2. Simulated annealing (SA) algorithm

In order to generalize the method and make it applicable to a wider range of structures, we use a SA like optimization method to find the match with the minimum total potential change. The pseudo-code of the SA algorithm is listed in Table 1. In each iteration, pairs of planes in the final state are switched. Two randomly chosen $\vec{q}_i$ and $\vec{b}_i$ values are switched and a new total potential change $\Delta W_{\text{total,new}}$ is found using the new arrangement. Using the Metropolis criterion, if $(\Delta W_{\text{total,new}} - \Delta W_{\text{total}}) < 0$, the switch is accepted. Otherwise, the switch may still be accepted, but with a certain probability. That is, a random number $u \in [0, 1)$ is generated. If $u \leq \exp((\Delta W_{\text{total}} - \Delta W_{\text{total,new}})/T)$ where T is a temperature variable, then the switch is accepted, otherwise, it is rejected. The value of T is decreased over time, after either every iteration or every a few iterations, to simulate cooling of the material. Table 1 lists the pseudo-code of the algorithm.

4.3.3. Plane constraints for strongly bonded pairs

In the cases where a pair of atoms has a bond that is much stronger than other bonds in the structure, as discussed in Section 4.2.2, some constraints must be placed on the corresponding planes to prevent the bond from breaking or elongating. Using Fig. 5 as a reference, the two horizontal planes must remain equidistant from each other throughout the transition. The distance between the two planes is kept unchanged and specified as

$$(\vec{a}_1 - \vec{a}_2) \cdot \vec{p}_1/|\vec{p}_1| = (\vec{b}_1 - \vec{b}_2) \cdot \vec{q}_1/|\vec{q}_1| \tag{14}$$

where $\vec{a}_1$ and $\vec{p}_1$ correspond to one plane and $\vec{a}_2$ corresponds to the other at the initial state, whereas $\vec{b}_1$, $\vec{q}_1$ and $\vec{b}_2$ correspond to the final state.

Table 1
Pseudo-code of the algorithm to search the correspondence of planes with the minimum potential change.

```
INPUT: initial points {ā_i}, final points {b̄_i}, initial vectors {p̄_i}, final vectors {q̄_i}, temperature T
OUTPUT: Combination of switches that yields the lowest ΔW_total
size = number of planes in the structure;
ΔT = Interval of temperature change;
ΔW_total = Σ_{i=1}^{size} (ΔU_i + ΔV_i);
WHILE (T > 0)
    m = random integer between 1 and size
    n = random integer between 1 and size
    q_1^(old) = q_m; q_2^(old) = q_n; b_1^(old) = b_m; b_2^(old) = b_n;
    q_n = q_1^(old); q_m = q_2^(old); b_n = b_1^(old); b_m = b_2^(old);
    ΔW_total,new = Σ_{i=1}^{size} (ΔU_i + ΔV_i);
    IF (ΔW_total,new − ΔW_total) > 0
        u = random number between 0 and 1;
      g = exp(−(ΔW_total,new − ΔW_total)/T);
        IF u > g
          q_m = q_1^(old); q_n = q_2^(old); b_m = b_1^(old); b_n = b_2^(old);
          ΔW_total,new = ΔW_total;
        END
    END
    ΔW_total = ΔW_total,new;
    T = T − ΔT;
END
```

Table 2
Extension of the pseudo-code in Table 1 for the plane constraint enforcement.

```
...
IF u > g OR p̄_1 · p̄_2 ≠ q̄_1 · q̄_2 OR p̄_3 · p̄_4 ≠ q̄_3 · q̄_4 OR
(ā_1 − ā_2) · p̄_1/|p̄_1| ≠ (b̄_1 − b̄_2) · q̄_1/|q̄_1|
          q_m = q_1^(old); q_n = q_2^(old); b_m = b_1^(old); b_n = b_2^(old);
          ΔW_total,new = ΔW_total;
END
...
```

Additionally, the angle between the two horizontal planes may remain constant. That is, for each pair of planes i and j, the condition

$$\vec{p}_i \cdot \vec{p}_j = \vec{q}_i \cdot \vec{q}_j \tag{15}$$

must be satisfied. For the searching process outlined in Section 4.3.2, the constraints in Eqs. (14) and (15) are enforced by rejecting any switch that does not meet the criteria. After a switch is made, we check if the resulting plane positions adhere to all of the constraints. If so, the process continues and $\Delta W_{\text{total,new}}$ is calculated. If not, the switch is rejected and a new combination is found. These constraints are further enforced as in the pseudo code in Table 2.

Plane-constrained structures, such as the graphite unit cell discussed in Section 4.2.2, have groups of atoms that remain in the same plane throughout the transition. The $\vec{p}_i$ that represents this plane in the initial state must transition to a specific $\vec{q}_i$ which represents that plane's location in the final state. If a switch is made that causes this plane to transition to a different location, that combination is rejected and a new switch is made.

5. Morphing of loci surface models

After the correspondence of periodic surfaces between the initial and final states is found, interpolation of surfaces is used to find the locations of each atom for a number of intermediate states. Each atom moves along a transition path to its final position in a predetermined number of steps. Interpolation is only applied to the surfaces, yielding a new set of surfaces at each step. Each atom location at any stage is found by the intersection of three surfaces.

A simple surface linear interpolation approach is used to define the intermediate basis vectors between the initial and final vectors by a linear interpolation between the two. Suppose that there are K stages during the morphing process. If a basis vector in the initial state (stage 1) is $\mathbf{p}_m^{(1)}$ and the corresponding one in the final state (stage K) is $\mathbf{p}_m^{(K)}$, then the basis vector $\mathbf{p}_m^{(k)}$ for the intermediate kth stage is given by

$$\mathbf{p}_m^{(k)} = (1 - \lambda^{(k)})\mathbf{p}_m^{(1)} + \lambda^{(k)}\mathbf{p}_m^{(K)} \quad (0 < \lambda^{(k)} < 1 \text{ for } k = 2, \ldots, K-1) \tag{16}$$

with the interpolation coefficients $\lambda^{(k)}$'s for all basis vectors $m = 1, \ldots, M$. Particularly, $\lambda^{(1)} = 0$ and $\lambda^{(K)} = 1$. The intervals of interpolation coefficients $\lambda^{(k)}$'s are chosen depending on how many intermediate states are desired.

The surface linear interpolation approach is a straightforward method for finding intermediate steps in a phase transition process. The positions of atoms during the transition are nonlinearly interpolated between initial and final states by the surface linear interpolation. Yet, the physical interaction between atoms is not captured when deciding their intermediate positions. Physical forces may prevent atoms from colliding or getting too close to each other. To model the physical interaction, a second approach, potential driven surface interpolation, is also proposed here. The physical forces between atoms are captured by the potential between surfaces. Given two surfaces

$$\psi_i(\mathbf{r}) = \sum_{l_i=1}^{L_i} \sum_{m_i=1}^{M_i} \mu_{l_i,m_i} \cos(2\pi\kappa_{l_i}(\mathbf{p}_{m_i} \cdot \mathbf{r})) = 0$$

and

$$\psi_j(\mathbf{r}) = \sum_{l_j=1}^{L_j} \sum_{m_j=1}^{M_j} \mu_{l_j,m_j} \cos(2\pi\kappa_{l_j}(\mathbf{p}_{m_j} \cdot \mathbf{r})) = 0$$

the pair-wise potential between them is defined as

$$E(\psi_i, \psi_j) = \sum_{l_j<l_i} \sum_{m_j<m_i} [\exp(|\mu_{l_i,m_i} - \mu_{l_j,m_j}| + (a_{m_i}a_{m_j} + b_{m_i}b_{m_j} + c_{m_i}c_{m_j})) \times \cos^2(\pi(\kappa_{l_i} + \kappa_{l_j})(\alpha_{m_i} - \alpha_{m_j}))]. \tag{17}$$

Eq. (17) combines the differences between the basis vectors and moments. Particularly, the lowest potential between two periodic planes that have the same normal direction is achieved when the distance in-between is the largest. That is, the two planes have a $\pi/2$ phase difference. Two perpendicular planes also have a relatively low potential.

Suppose that there are a total of N surfaces in a model. The potential driven surface interpolation approach individually finds the interpolation coefficient $\lambda_i^{(k)}$ for the ith surface at the kth stage, instead of the predetermined $\lambda^{(k)}$'s for all surfaces. The process is to find $\lambda_i^{(k)}$'s such that the total pair-wise potential for all surfaces at the kth stage is minimized. That is, we need to solve

$$\min_{\lambda_1^{(k)},\ldots,\lambda_N^{(k)}} \sum_{i=1}^{N}\sum_{j=i+1}^{N} E(\psi_i^{(k)}(\lambda_i^{(k)}), \psi_j^{(k)}(\lambda_j^{(k)})) \quad \text{for } k = 2, \ldots, K$$

s.t.

$$\text{(C1)} \sum_{i=1}^{N} \lambda_i^{(k)} = N\lambda^{(k)} \tag{18}$$

$$\text{(C2)}\ \lambda_i^{(1)} = 0 \quad \text{and} \quad \lambda_i^{(k-1)} - \varepsilon \le \lambda_i^{(k)} \le 1 \quad (i = 1, \ldots, N).$$

Notice that the intermediate surface $\psi_i^{(k)}$ at stage k is a function of $\lambda_i^{(k)}$ where its corresponding basis vectors are calculated similar to Eq. (16). The equality constraint C1 is the boundary condition that the initial and final stages are met. At the same time, it ensures that the system evolves by stages with the predetermined values of $\lambda^{(k)}$'s. The lower and upper bound constraint C2 ensures that the system evolves forward in general, where a small number ε is introduced in the lower bound such that a limited setback is allowed to have more stable intermediate states with a lower potential level.

6. Demonstration and validation

In this section, we demonstrate the proposed loci-surface guided transition path search methods by examples of iron–titanium (FeTi), vanadium dioxide (VO_2), and iron—platinum (FePt) phase transition. FeTi is being extensively studied as a candidate material for hydrogen storage applications. VO_2 thin films undergo changes during reversible and ultra-fast metal-to-semiconductor phase transition, which can be widely applied in high-volume rewritable holographic storage, high-speed fiber-optical switching, smart windows, etc. The layered state of FePt exhibits high magnetocrystalline anisotropy, making it potentially useful as a material in the high density data storage. In order to search saddle points on the PES by methods such as the NEB, a good initial guess is required. The proposed geometry-guided path search method provides such an initial guess that is close to the minimum energy path.

6.1. FeTi +H transition

FeTi experiences transition from a body-centric structure to an orthorhombic state where it can hold two hydrogen (H) atoms. Fig. 6(a) shows four unit cells of the FeTi structure at its initial state. The unit cell of FeTi is body-centered cubic, where the Ti atoms are at the center and Fe atoms at the corners. The size of the unit cell is $a = b = c = 5.629$ bohr [47]. Fig. 6(b) shows one of the possible final states when two H atoms are absorbed in each unit cell forming the structure of FeTiH. This is an orthorhombic structure with Fe and Ti atoms on each face. Fe atoms still occupy the corners as well as the centers of the top and bottom faces. Ti atoms are located in the center of each side face. H atoms are located on two side faces. The size of the unit cell is $a = 5.586$ bohr, $b = 8.585$ bohr, and $c = 8.292$ bohr [47]. Notice that Fig. 6(b) shows two unit cells of FeTiH, which correspond to four unit cells of FeTi.

Geometry optimization or relaxation based on the ab initio molecular dynamics (CPMD) is performed first on both initial and final states of the FeTi + H transition using the software tool Quantum-Espresso [48]. Since searching the saddle point of the transition process where H atoms are absorbed, requires us to have the same number of atoms in a unit cell, H atoms are introduced into the body-centered cubic FeTi structure to match the final FeTiH structure. As shown in Fig. 7, there are two basis atoms for each type of Fe, Ti, and H in one unit cell of FeTiH as the final structure. Correspondingly, for two unit cells of the body-centered FeTi, there are two Fe atoms and two Ti atoms as the basis of the initial structure, in addition to the two H atoms. In the initial structure, there is a H atom placed on the side of each unit cell, which is one of the most likely positions where H atoms are first absorbed in the cell [49]. The size of the unit cell for the initial structure is also set to be the size of the final structure, where a meta-stable structure is likely to form. After the geometry optimization, meta-stable structures with the local minimum total energy are found, which are very close to the ones in Fig. 7.

During the search of the initial transition path, atom locations for a unit cell of the two states in Fig. 7 are compared using the method described in Section 4.2. For each atom in the initial state, the corresponding location in the final state is found based on Eq. (10). Three planes are defined for each atom in the initial or final state. The respective y–z, x–z, and x–y planes of atom i are

$$\begin{cases} \psi_i^{yz}(x) = \cos(\pi(x + a/2 + x_i)/2) = 0 \\ \psi_i^{xz}(y) = \cos(\pi(y + b/2 + y_i)/2) = 0 \\ \psi_i^{xy}(z) = \cos(\pi(z + c/2 + z_i)/2) = 0 \end{cases}$$

where $a = 5.586$, $b = 8.585$, and $c = 8.292$ define the size of the unit cell, and x_i, y_i, and z_i are the coordinates of the six atoms.

Face correlation as described in Section 4.2.2 is used to reduce the number of loci planes. If we assume that the two basis Fe atoms are always on the same vertical y–z plane during the transition, the total number of planes is reduced from 18 to 17. Similarly, if the two Ti atoms and two H atoms are always on the same y–z plane respectively, the number of planes is further reduced to 15.

By the surface linear interpolation in Eq. (16), the basis vectors of the planes that define the atom positions in the initial and final states, and the basis vectors for planes in the intermediate states can be found. The PS models in Fig. 8 represent six different states during the phase transition. Two unit cells of FeTi morph to one unit cell of FeTiH. It can be seen that the basis H atom on the right moves up while the basis H atom on the left moves down. At the same time, the basis Fe atom in the middle moves down towards the center of the face, while the basis Fe atom in the corner shifts right. For the two basis Ti atoms, the left one moves up to the top face while the right one moves further out of the unit cell.

Using the potential-driven surface interpolation in Eq. (18), we receive a different initial guess of the transition path, as shown in Fig. 9. Compared to the previous one in Fig. 8, atoms tend to move individually one after another instead of simultaneously. Table 3 shows the detailed interpolation coefficients $\lambda_i^{(k)}$'s for each plane at each stage as a result of minimizing potentials.

The initial guess of the transition path in Fig. 8 is imported as the input of the NEB method in Quantum-Espresso to find the MEP. The result is shown in Fig. 10, where each image at the bottom of the figure represents a state with a total of six. The initial and final states are the respective ones in Fig. 8, whereas the other four intermediate ones have been updated to reflect the MEP. The calculated energy level for each state is shown with the solid lines. Particularly, image 3, corresponding to −4713.9203

Table 3
Interpolation coefficients for y–z, x–z, x–y planes as the result of the potential-driven surface interpolation in Fig. 9.

	$k=1$			$k=2$			$k=3$			$k=4$			$k=5$			$k=6$		
	y–z	x–z	x–y	y–z	x–z	x–y	y–z	x–z	x–y	y–z	x–z	x–y	y–z	x–z	x–y	y–z	x–z	x–y
Fe	0	0	0	0	0	0	1	0.9837	0.6394	0.9995	0.9979	0.9963	0.9995	0.9999	0.9992	1	1	1
Fe	0	0	0	0.6409	0	0.4990	0.6555	0	0.5000	0.9968	0	0.7783	0.9998	0.1684	0.7773	1	1	1
Ti	0	0	0	0.0146	0	0.4990	0.3269	0	0.4984	0.9970	0	0.9970	1	0.6723	1	1	1	1
Ti	0	0	0	0	0.4834	0	0	0.4824	0	0. 2289	0.4814	0.5361	1	0.6723	0.9994	1	1	1
H	0	0	0	0	0.4990	0	0	0.4980	0	0	0.5361	0	0.7328	0.6723	0.6723	1	1	1
H	0	0	0	0.4990	0.4912	0	0.4980	0.4902	0.3269	0.5361	0.4892	0.5361	0.6723	0.6723	0.6723	1	1	1

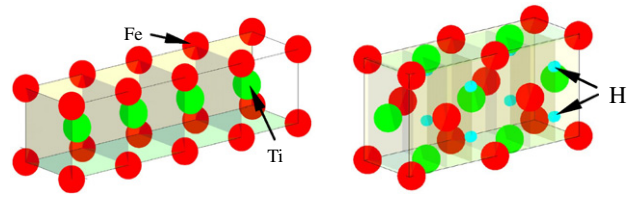

(a) FeTi. (b) FeTiH.

Fig. 6. Comparison between FeTi and FeTiH.

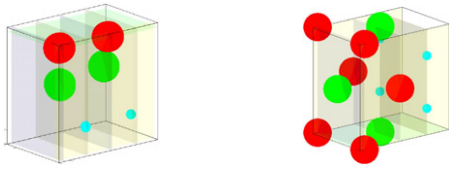
(a) FeTi + H initial structure. (b) FeTiH final structure.

Fig. 7. Initial and final phases of FeTi with H absorbed.

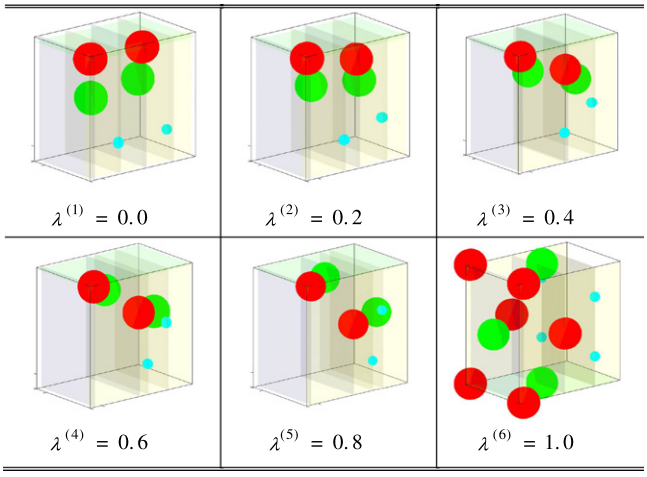

Fig. 8. Initial guess of the transition path for FeTi + H based on the surface linear interpolation in Eq. (16).

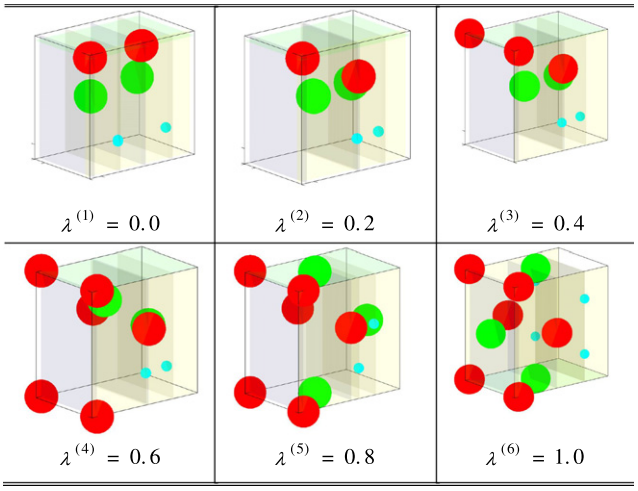

Fig. 9. Initial guess of the transition path for FeTi + H based on the potential-driven surface interpolation in Eq. (18).

eV, has the highest energy level along the MEP. It is the saddle point found by the NEB method. The activation energy is 1.5771 eV, which corresponds to 0.26285 eV per atom. The second initial guess of transition path in Fig. 9 from the potential-driven surface interpolation is also used to run the NEB. The resultant MEP is shown as the dash lines in Fig. 10. The corresponding images are shown at the top of the figure. It is seen that the MEP found by the initial guess from the potential-driven surface interpolation gives a saddle point energy value of −4708.5716. The activation energy found is 6.9258 eV, which corresponds to 1.1543 eV per atom. This is a higher energy level of the saddle point than the one from the surface linear interpolation. The lower energy saddle point reflects the true MEP better. In contrast, we also run the NEB method with its empirical default initial guess, which is the simple linear interpolation of atom positions. The result is also shown in Fig. 10, represented as the dotted lines. In this case, the NEB method fails in searching the saddle point after 100 NEB iterations, since there is no intermediate state that has a higher energy level than both the initial and final states. Total CPU time required for the potential-driven method was 34 h on a computer node with four CPUs, while the linear interpolation method required 14.5 h. Experimentally, the activation energy for this material has been found to be 0.2912 eV per atom [50], which is very close to the result obtained with the surface linear interpolation method.

It can be seen from the results in Fig. 10 that both proposed methods are superior to the default empirical initial guess, which fails to find the saddle point in this case. It is also observed that our more involved, potential-driven surface interpolation method generates poorer results than the simpler linear interpolation method, as the resulting saddle point energy level is higher. One possible explanation for this result is that for the predicted intermediate states of the potential-driven interpolation method, as seen in Fig. 9, the atoms move individually, rather than simultaneously as in Fig. 8. The individual movement or single-hop diffusion sometimes requires a greater amount of energy than the coordinated diffusion, which has been discovered by first-principles simulations and experimentally observed (e.g. [51,52]). Here, the linear interpolation method may provide a more accurate prediction of the atom movement and therefore generate a better result in terms of saddle point energy levels. However, the potential driven surface interpolation method still provides more flexibility and a different guess of transition path; it also avoids paths which may result in atom collisions, which could be an important consideration.

6.2. VO_2 transition

To demonstrate the process outlined in Section 4.3, we will use an example of VO_2 transition. The initial rutile phase and final M_2

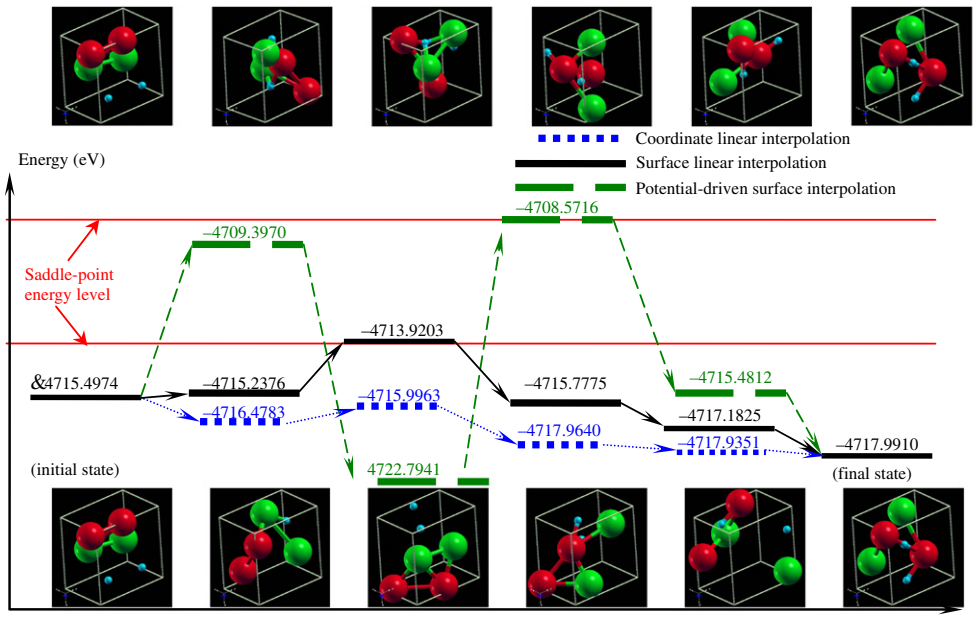

Fig. 10. Results of MEP in FeTi + H transition by the NEB method with different initial guesses.

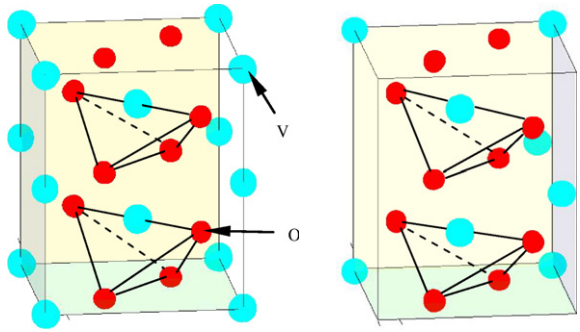

(a) VO_2 initial rutile phase. (b) VO_2 final M_2 phase.

Fig. 11. Initial and final phases of VO_2.

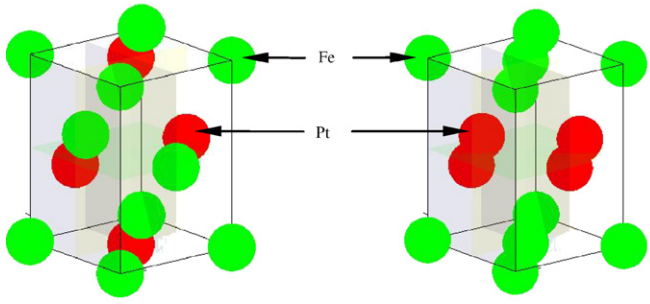

(a) FePt initial A1 phase (b) FePt final $L1_0$ phase

Fig. 12. Initial and final phases of FePt.

phase of VO_2 are shown in Fig. 11. In each unit cell, there are eight oxygen (O) basis atoms. Following the procedure in Section 4.1, we build two tetrahedrons or eight different planes for each phase so that the positions of the O atoms can be uniquely determined by the intersections of the eight planes. Setting the values of c and s in Eqs. (11) and (12) to be at least 300, we can reliably find the correct correspondence of the periodic planes between the initial and final stages, where the minimum total potential change $\Delta W_{\text{total}} = 447.35$ is found.

Similar to the previous example in Section 6.1, the surface linear interpolation method is used to find the initial guess of the transition path. After the NEB search, the respective energy levels for seven images are: (1) −5006.1158 eV, (2) −5000.6632 eV, (3) −5003.8746 eV, (4) −4997.6627 eV, (5) −4990.0234 eV, (6) −4989.7258 eV, and (7) −5006.4782 eV. Image (6) has the highest energy and therefore represents the saddle point. The activation energy found is 16.39 eV, which corresponds to 1.37 eV per atom. The experimental data for the activation energy is approximately 0.6 eV per atom [53]. Using the empirical default initial guess, the NEB fails to locate the saddle point again.

6.3. FePt transition

The unit cell of the initial disordered A1 state of FePt is face centered cubic with two iron (Fe) and two platinum (Pt) atoms each. The structure transitions into a layered $L1_0$ face centered tetragonal phase, where atoms of the same species are located in the same plane. Both phases are shown in Fig. 12. In the final phase, the dimensions of the unit cell are $a = 3.874$ bohr and $c = 3.714$ bohr [54]. Similar to the previous examples, the surface linear interpolation is used to generate an initial guess of atom locations during the transition, where the activation energy found is 0.8099 eV per atom. The result from the empirical default initial guess is 0.7602 eV per atom. Both are reasonably close to the experimentally measured 1.7 eV per atom [55].

7. Concluding remarks

In this paper, we proposed a geometry-guided phase transition pathway search method for finding intermediate states in the phase transition of crystals. A periodic surface model is used to build crystals parametrically for ease of construction and modification. The transition pathway is then estimated by interpolation of periodic planes, and atom positions are determined by intersection of the loci surfaces. The estimation can provide a good initial guess of MEP for physics-based transition path and saddle point search methods such that the risk of being trapped in a local minimum energy path is reduced. To enable this integrated computer-aided transition pathway design, we developed methods of finding the correspondence of atom locations and periodic planes in the initial and final states of a crystalline material's unit cell. A heuristic

global optimization approach is taken to reduce the complexity of searching correspondence. Once the surface models in the initial and final states are matched, the developed surface linear interpolation and potential-driven surface interpolation are used to make predictions about where each atom will move.

The proposed approach is intended to integrate geometry and physics information in materials modeling and simulation. Further exploration of the intrinsic relation between the two that goes beyond the simple observations is meaningful. Observations from this paper include that geometric structures and physical properties in nanoscale materials have connections or even one-to-one mappings. Metamorphosis in geometry can integrate more physics of phase transitions. Structures with strongly bonded atoms can simplify the computation of geometric morphing. Modeling the interactions among geometric entities can help simulate physical phenomena more efficiently.

Numerical error is a challenge in our proposed approach. When the angles between intersecting planes are small and rotation is involved during the surface interpolation, the numerical error to compute intersections may become significant. The discretization of the 3D space to generate fine-grained models in our implicit modeling scheme is then essential to keep errors small, which will increase the computational time. One possible way to alleviate this is to define planes with intersecting angles as large as possible, such as the y–z, x–z, and x–y planes. In this paper we have shown that for some cases the saddle point is identified more accurately using our techniques. In future research, we would like to extend them to more applications and test how effective our methods are, with opportunities to further refine our approach.

Acknowledgments

This work is supported in part by the NSF grant CMMI-1001040.

References

[1] Wang Y. Periodic surface modeling for computer aided nano design. Computer-Aided Design 2007;39(3):179–89.
[2] Qi C, Wang Y. Feature-based crystal construction with periodic surfaces. Computer-Aided Design 2009;41(11):792–800.
[3] Wang Y. Loci periodic surface reconstruction from crystals. Computer-Aided Design & Applications 2007;4(1–4):437–47.
[4] Wang Y. Degree elevation and reduction of periodic surfaces. Computer-Aided Design & Applications 2008;5(6):841–54.
[5] Wang Y. Computing Minkowski sums of periodic surface models. Computer-Aided Design & Applications 2009;6(6):825–37.
[6] Qi C, Wang Y. Metamorphosis of periodic surface models. In: Proceedings of 2009 ASME IDETC/CIE, Paper No. DETC2009/DAC-87101, 2009.
[7] Yeomans JM. Statistical mechanics of phase transitions. New York: Oxford University Press; 2002.
[8] Papon P, Leblond J, Meijer PHE. The physics of phase transitions: concepts and applications. Berlin: Springer-Verlag; 2006.
[9] Lavrov AN, Komiya S, Ando Y. Antiferromagnets: magnetic shape-memory effects in a crystal, Nature, 418, p. 385–6.
[10] Mnyukh Y. Fundamentals of solid-state phase transitions, ferromagnetism and ferroelectricity, 1 st Books Library 2001.
[11] Cerjan C, Miller W. On finding transition states. Journal of Chemical Physics 1981;75:2800–6.
[12] Dewar MJS, Healy EF, Stewart JJP. Location of transition states in reaction mechanisms. Journal of Chemical Society, Faraday Transactions 1984;2(80):52–7.
[13] Edelsbrunner H. Deformable smooth surface design. Discrete & Computational Geometry 1999;21(1):87–115.
[14] Edelsbrunner H. Surface reconstruction by wrapping finite point sets in space. In: Discrete and Computation Geometry. The Goodman–Pollack Festschrift; 2003. p. 379–404.
[15] Bajaj C, Pascucci V, Shamir A, Holt R, Netravali A. Dynamic maintenance and visualization of molecular surfaces. Discrete Applied Mathematics 2003;127(1):23–51.
[16] Zhang Y, Xu G, Bajaj C. Quality meshing of implicit solvation models of biomolecular structures. Computer-Aided Geometric Design 2006;23(6):510–30.
[17] Ryu J, Park R, Kim D-S. Molecular surfaces on proteins via beta shapes. Computer Aided Design 2007;39(12):1042–57.
[18] Ryu J, Cho Y, Kim D-S. Triangulation of molecular surfaces. Computer Aided Design 2009;41(6):463–78.
[19] Kim D-S, Cho Y, Sugihara K, Ryu J, Kim D. Three-dimensional beta-shapes and beta-complexes via quasi-triangulation. Computer Aided Design 2010;42(10):911–29.
[20] Au CK, Woo TC. Ribbons: their geometry and topology. Computer-Aided Design & Applications 2004;1(1–4):1–6.
[21] Kim D-S, Cho Y, Kim D. Euclidean Voronoi diagram of 3D balls and its computation via tracing edges. Computer-Aided Design 2005;37(13):1412–24.
[22] Bajaj C. A Laguerre Voronoi based scheme for meshing particle swarms. Japan Journal of Industrial and Applied Mathematics 2005;22(2):167–77.
[23] Jonsson H, Mills G, Jacobsen K. Classical and quantum dynamics in condensed phase simulations. Hackensack (NJ): World Scientific; 1998. p. 385–404 [Chapter 16].
[24] Henkelman G, Jonsson H. Improved tangent estimate in the nudged elastic band method for finding minimum energy paths and saddle points. Journal of Chemical Physics 2000;113(22):9978–85.
[25] Trygubenko S, Wales D. A doubly nudged elastic band method for finding transition states. Journal of Chemical Physics 2004;120(5):2082–94.
[26] Zhu T, Li J, Samanta A, Kim HG, Suresh S. Interfacial plasticity governs strain rate sensitivity and ductility in nanostructured metals. Proceedings of the National Academy of Sciences of the USA 2007;104(9):3031–6.
[27] Henkelman G, Uberuaga BP, Jonsson H. A climbing image nudged elastic band method for finding saddle points and minimum energy paths. Journal of Chemical Physics 2000;113(22):9901–4.
[28] Galvan I, Field M. Improving the efficiency of the NEB reaction path finding algorithm. Journal of Computational Chemistry 2008;29(1):139–43.
[29] Weinan E, Ren W, Vanden-Ejinden E. String method for the study of rare events. Physical Review B 2002;66(5):052301 [1–4].
[30] Ren W. Higher order string method for finding minimum energy path. Commun. Math. Sci. 2003;1(2):377–84.
[31] Peters B, Heyden A, Bell AT, Chakraborty A. A growing string method for determining transitions states: comparison to the nudged elastic band and string methods. Journal of Chemical Physics 2004;120(7):7877–86.
[32] Burger S, Yang W. Quadratic string method for determining the minimum-energy path based on multiobjective optimization. Journal of Chemical Physics 2006;124(5):054109 [1–12].
[33] Chen L, Ying C, Ala-Nissila T. Finding transition paths and rate coefficients through accelerated Langevin dynamics. Physical Review E 2002;65(4):042101 [1–4].
[34] Fischer S, Karplus M. Conjugate Peak Refinement: an algorithm for finding reaction paths and accurate transition states with many degrees of freedom. Chemical Physics Letters 1992;194(3):252–61.
[35] Dey B, Ayers P. A Hamilton–Jacobi type equation for computing minimum potential energy paths. Molecular Physics 2006;104(4):541–58.
[36] Simons J, Joergensen P, Taylor H, Ozment J. Walking on potential energy surfaces. Journal of Physical Chemistry 1983;87(15):2745–53.
[37] Banerjee A, Adams N, Simons J, Shepard R. Search for stationary points on surfaces. Journal of Physical Chemistry 1985;89(1):52–7.
[38] Ionova IV, Carter EA. Ridge method for finding saddle points on potential energy surfaces. Journal of Chemical Physics 1993;98(8):6377–86.
[39] Henkelman G, Jonsson H. A dimer method for finding saddle points on high dimensional potential surfaces using only first derivatives. Journal of Chemical Physics 1999;111(15):7010–22.
[40] Quapp W, Hirsch M, Imig O, Heidrich D. Searching for saddle points of a potential energy surface by following a reduced gradient. Journal of Computational Chemistry 1998;19(9):1087–100.
[41] Anglada JM, Besalu E, Bofill JM, Crehuet R. On the quadratic reaction path evaluated in a reduced potential energy surface model and the problem to locate transition states. Journal of Computational Chemistry 2001;22(4):387–406.
[42] Govind N, Petersen M, Fitzgerald G, King-Smith D, Andzelm J. A generalized synchronous transit method for transition state location. Computational Materials Science 2003;28(2):250–8.
[43] Dewar MJS, Healy EF, Stewart JJP. Location of transition states in reaction mechanisms. Journal of Chemical Society, Faraday Transactions 1984;2(80):227.
[44] Mousseau N, Barkema GT. Traveling through potential energy landscapes of disordered materials: the activation–relaxation technique. Physical Review E 1998;57(2):2419–24.
[45] Miron RA, Fichthorn KA. The step and slide method for finding saddle points on multidimensional potential surfaces. Journal of Chemical Physics 2001;115(19):8742–7.
[46] Lin Y, Stadtherr MA. Locating stationary points of Sorbate–Zeolite potential energy surfaces using interval analysis. Journal of Chemical Physics 2004;121(20):10159–66.
[47] Kinaci A, Aydinol MK. Ab initio investigation of FeTi–H system. International Journal of Hydrogen Energy 2007;32(13):2466–74.
[48] Giannozzi P, Baroni S, Bonini N, Calandra M, Car R, Cavazzoni C, Ceresoli D, Chiarotti G, Cococcioni M, Dabo I, Dal Corso A, Fabris S, Fratesi G, De Gironcoli S, Gebauer R, Gerstmann U, Gougoussis C, Kokalj A, Lazzeri M, Martin-Samos L, Marzari N, Mauri F, Mazzarello R, Paolini S, Pasquarello A, Paulatto L, Sbraccia C, Scandolo S, Sclauzero G, Seitsonen AP, Smogunov A, Umari P, Wentzcovitch RM. Quantum Espresso: a modular and open-source

software project for quantum simulations of materials. Journal of Physics: Condensed Matter 2009;21(39):395502 [1–19].
[49] Izanlou A, Aydinol MK. An ab initio study of dissociative adsorption of H_2 on FeTi surfaces. International Journal of Hydrogen Energy 2010;35(4): 1681–92.
[50] Sen FG, Kinaci A, Aydinol MK. Effect of alloying elements on the formation of FeTiH: an ab initio study. In: Baranowski B, Zaginaichenko SY, Schur DV, Skorokhod VV, Veziroglu A, editors. Carbon nanomaterials in clean energy hydrogen systems. Netherlands: Springer; 2009. p. 573–8.
[51] Bogicevic A, Hyldgaard P, Wahnstrom G, Lundqvist B. Al dimer dynamics on Al(111). Physical Review Letters 1998;81(1):172–5.
[52] Stumpf R, Scheffler M. Theory of self-diffusion at and growth of Al(111). Physical Review Letters 1993;72(2):254–7.
[53] Berglund CN, Guggenheim HJ. Electronic properties of VO_2 near the semiconductor–metal transition. Physical Review 1969;185(3):1022–33.
[54] Barmak K, Kim J, Lewis LH, Coffey KR, Toney MF, Kellock AJ, Thiele J-U. On the relationship of magnetocrystalline anisotropy and stoichiometry in epitaxial $L1_0$ CoPt (001) and FePt (001) thin films. Journal of Applied Physics 2005;98(3): 033904 [1–10].
[55] Barmak K, Kim J, Shell S, Svedberg EV, Howard JK. Calorimetric studies of the A1 to $L1_0$ transformation in FePt and CoPt thin films. Applied Physics Letters 2002;80(22):4268–70.

Please cite this article in press as: Crnkic E, et al. Geometry guided crystal phase transition pathway search. Computer-Aided Design (2011), doi:10.1016/j.cad.2011.08.009